RegCM Version 4.0
User's Guide

Nellie Elguindi, Xunqiang Bi, Filippo Giorgi, Badrinath Nagarajan,
Jeremy Pal, Fabien Solmon, Sara Rauscher, and Ashraf Zakey

Trieste, Italy
June 2010

Acknowledgements

This paper is dedicated to those that have contributed to the growth of RegCM system over the past 20+ years, the members (800+) of the RegCNET, and the ICTP.

Abstract

As one of the main aims of the Abdus Salam International Centre for Theoretical Physics (ICTP) is to foster the growth of advanced studies and research in developing countries, the main purpose of this Regional Climate Model (REGional Climate Model (RegCM)) Tutorial Class Notes is to give model users a guide to learn the whole RegCM Model System.

The RegCM Tutorial Class is offered as a part of extended hands-on lab sessions during a series of Workshops organized by the Physics of Weather and Climate (PWC) group at the ICTP.

RegCM was originally developed at the National Center for Atmospheric Research (NCAR) and has been mostly applied to studies of regional climate and seasonal predictability around the world. The workshop participants are welcome to use RegCM for regional climate simulation over different areas of interest. The RegCM is available on the World Wide Web at **https://eforge.escience-lab.org/gf/project/regcm/wiki/**.

Contents

1 Introduction **6**
1.1 History . . . 6
1.2 The RegCM Model Horizontal and Vertical Grid . . . 7
1.3 Map Projections and Map-Scale Factors . . . 9

2 Model Description **10**
2.1 Dynamics . . . 10
2.2 Physics . . . 12
2.2.1 Radiation Scheme . . . 12
2.2.2 Land Surface Models . . . 12
2.2.3 Planetary Boundary Layer Scheme . . . 15
2.2.4 Convective Precipitation Schemes . . . 15
2.2.5 Large-Scale Precipitation Scheme . . . 17
2.2.6 Ocean flux Parameterization . . . 18
2.2.7 Prognostic Sea Surface Skin Temperature Scheme . . . 18
2.2.8 Pressure Gradient Scheme . . . 18
2.2.9 Lake Model . . . 18
2.2.10 Aerosols and Dust (Chemistry Model) . . . 19

List of Figures

1 Schematic representation of the vertical structure of the model. This example is for 16 vertical layers. Dashed lines denote half-sigma levels, solid lines denote full-sigma levels. (Adapted from the PSU/NCAR Mesoscale Modeling System Tutorial Class Notes and User's Guide.) 7
2 Schematic representation showing the horizontal Arakawa B-grid staggering of the dot and cross grid points. 8

List of Tables

1 Land Cover/Vegetation classes 13
2 BATS vegetation/land-cover 14
3 Resolution for CLM input parameters 15

1 Introduction

1.1 History

The idea that limited area models (LAMs) could be used for regional studies was originally proposed by *Dickinson et al.* [1989] and *Giorgi* [1990]. This idea was based on the concept of one-way nesting, in which large scale meteorological fields from General Circulation Model (GCM) runs provide initial and time-dependent meteorological lateral boundary conditions (LBCs) for high resolution Regional Climate Model (RCM) simulations, with no feedback from the RCM to the driving GCM.

The first generation NCAR RegCM was built upon the NCAR-Pennsylvania State University (PSU) Mesoscale Model version 4 (MM4) in the late 1980s [*Dickinson et al.*, 1989; *Giorgi*, 1989]. The dynamical component of the model originated from the MM4, which is a compressible, finite difference model with hydrostatic balance and vertical σ-coordinates. Later, the use of a split-explicit time integration scheme was added along with an algorithm for reducing horizontal diffusion in the presence of steep topographical gradients [*Giorgi et al.*, 1993a, b]. As a result, the dynamical core of the RegCM is similar to that of the hydrostatic version of Mesoscale Model version 5 (MM5) [*Grell et al.*, 1994].

For application of the MM4 to climate studies, a number of physics parameterizations were replaced, mostly in the areas of radiative transfer and land surface physics, which led to the first generation RegCM [*Dickinson et al.*, 1989; *Giorgi*, 1990]. The first generation RegCM included the Biosphere-Atmosphere Transfer Scheme, BATS, [*Dickinson et al.*, 1986] for surface process representation, the radiative transfer scheme of the Community Climate Model version 1 (CCM1), a medium resolution local planetary boundary layer scheme, the Kuo-type cumulus convection scheme of [*Anthes*, 1977] and the explicit moisture scheme of [*Hsie et al.*, 1984].

A first major upgrade of the model physics and numerical schemes was documented by [*Giorgi et al.*, 1993a, b], and resulted in a second generation RegCM, hereafter referred to as REGional Climate Model version 2 (RegCM2). The physics of RegCM2 was based on that of the NCAR Community Climate Model version 2 (CCM2) [*Hack et al.*, 1993], and the mesoscale model MM5 [*Grell et al.*, 1994]. In particular, the CCM2 radiative transfer package [*Briegleb*, 1992] was used for radiation calculations, the non local boundary layer scheme of [*Holtslag et al.*, 1990] replaced the older local scheme, the mass flux cumulus cloud scheme of [*Grell*, 1993] was added as an option, and the latest version of BATS1E [*Dickinson et al.*, 1993] was included in the model.

In the last few years, some new physics schemes have become available for use in the RegCM, mostly based on physics schemes of the latest version of the Community Climate Model (CCM), Community Climate Model version 3 (CCM3) [*Kiehl et al.*, 1996]. First, the CCM2 radiative transfer package has been replaced by that of the CCM3. In the CCM2 package, the effects of H_2O, O_3, O_2, CO_2 and clouds were accounted for by the model. Solar radiative transfer was treated with a δ-Eddington approach and cloud radiation depended on three cloud parameters, the cloud fractional cover, the cloud liquid water content, and the cloud effective droplet radius. The CCM3 scheme retains the same structure as that of the CCM2, but it includes new features such as the effect of additional greenhouse gases (NO_2, CH_4, CFCs), atmospheric aerosols, and cloud ice.

The other primary changes are in the areas of cloud and precipitation processes. The original explicit moisture scheme of *Hsie et al.* [1984] has been substituted with a simplified version because the original scheme was computationally too expensive to be run in climate mode. In the simplified scheme only a prognostic equation for cloud water is included, which accounts for cloud water formation, advection and mixing by turbulence, re-evaporation in sub-saturated conditions, and conversion into rain via a bulk autoconversion term. The main novelty of this scheme does not reside of course in the simplistic microphysics, but in the fact that the prognosed cloud water variable is directly used in the cloud radiation calculations. In the previous versions of the model, cloud water variables for radiation calculations were diagnosed in terms of the local relative humidity. This new feature adds a very important and far reaching element of interaction between the simulated hydrologic cycle and energy budget calculations.

Changes in the model physics include a large-scale cloud and precipitation scheme which accounts for the subgrid-scale variability of clouds [*Pal et al.*, 2000], new parameterizations for ocean surface fluxes [*Zeng et al.*, 1998], and a cumulus convection scheme [*Emanuel*, 1991; *Emanuel and Zivkovic-Rothman*, 1999]. Also new in the model is a mosaic-type parameterization of subgrid-scale heterogeneity in topography and land use [*Giorgi et al.*, 2003b]. Other improvements in RegCM3 involve the input data. The USGS Global Land Cover Characterization and Global 30 Arc-Second Elevation datasets are now used to create the terrain files. In addition, NCEP and ECMWF global reanalysis datasets are used for the intial and boundary conditions. Lastly, improvements in the user-friendliness of the model have been made. New scripts have been included which make running the programs

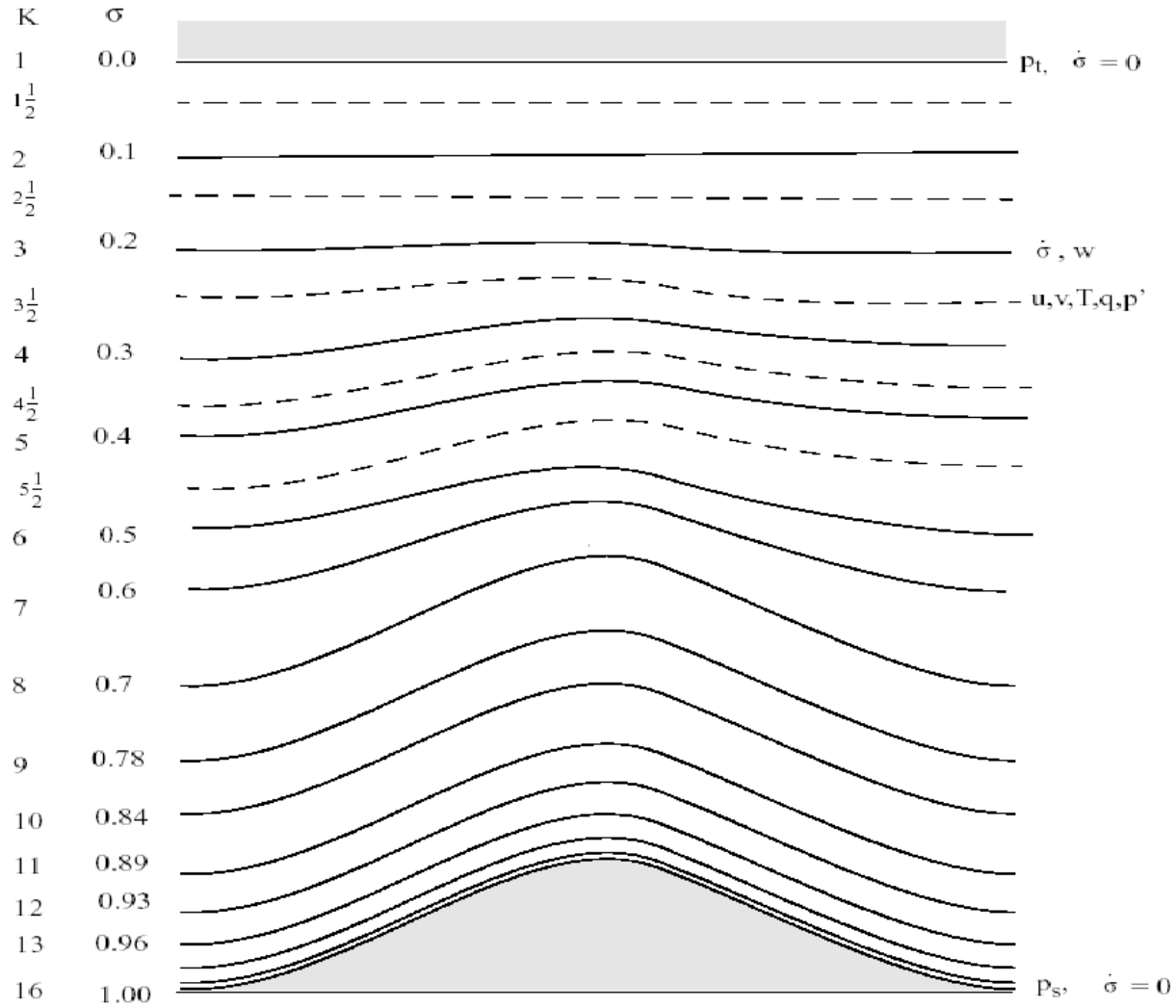

Figure 1: Schematic representation of the vertical structure of the model. This example is for 16 vertical layers. Dashed lines denote half-sigma levels, solid lines denote full-sigma levels. (Adapted from the PSU/NCAR Mesoscale Modeling System Tutorial Class Notes and User's Guide.)

easier. Also, a new website has been developed where users can freely download the entire RegCM system, as well as all of the input data necessary for a simulation.

The RegCM modeling system has four components: Terrain, ICBC, RegCM, and Postprocessor. Terrain and ICBC are the two components of RegCM preprocessor. Terrestrial variables (including elevation, landuse and sea surface temperature) and three-dimensional isobaric meteorological data are horizontally interpolated from a latitude-longitude mesh to a high-resolution domain on either a Rotated (and Normal) Mercator, Lambert Conformal, or Polar Stereographic projection. Vertical interpolation from pressure levels to the σ coordinate system of RegCM is also performed. σ surfaces near the ground closely follow the terrain, and the higher-level σ surfaces tend to approximate isobaric surfaces.

Since the vertical and horizontal resolution and domain size can vary, the modeling package programs employ parameterized dimensions requiring a variable amount of core memory, and the requisite hard-disk storage amount is varied accordingly.

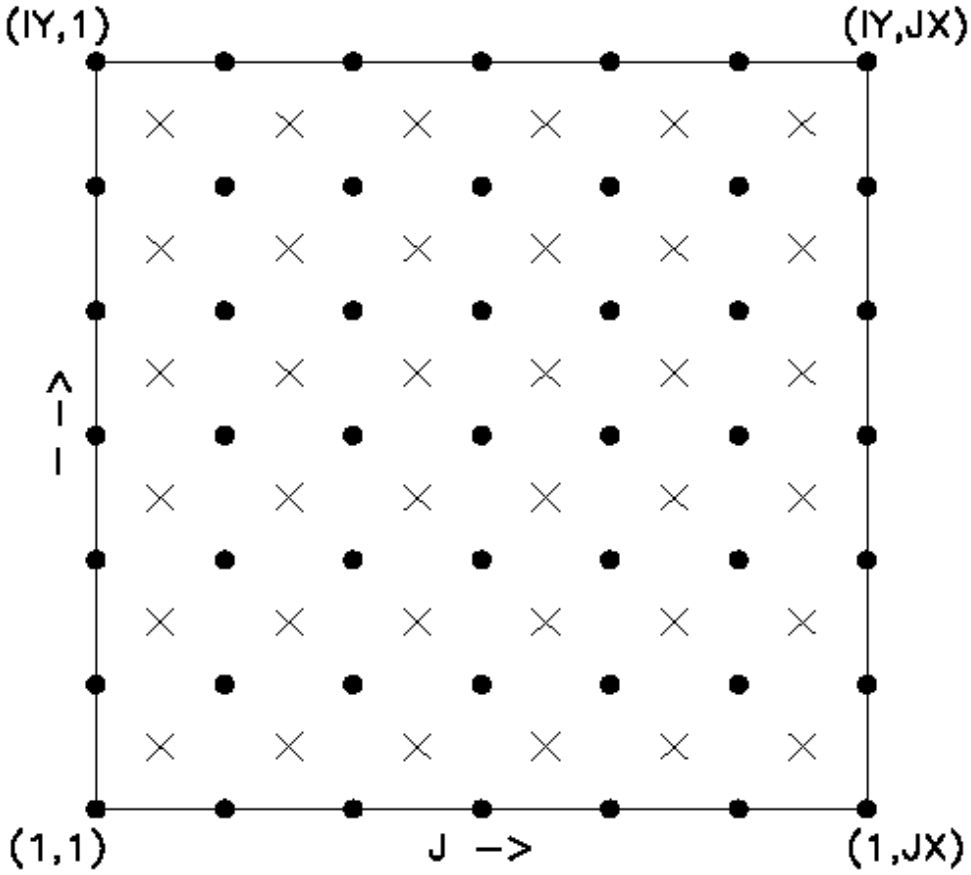

Figure 2: Schematic representation showing the horizontal Arakawa B-grid staggering of the dot and cross grid points.

1.2 The RegCM Model Horizontal and Vertical Grid

It is useful to first introduce the model's grid configuration. The modeling system usually gets and analyzes its data on pressure surfaces, but these have to be interpolated to the model's vertical coordinate before input to the model. The vertical coordinate is terrain-following (Figure 1) meaning that the lower grid levels follow the terrain while the upper surface is flatter. Intermediate levels progressively flatten as the pressure decreases toward the top of the model. A dimensionless σ coordinate is used to define the model levels where p is the pressure, p_t is a specified constant top pressure, p_s is the surface pressure.

$$\sigma = \frac{(p - p_t)}{(p_s - p_t)} \tag{1}$$

It can be seen from the equation and Figure 1 that σ is zero at the top and one at the surface, and each model level is defined by a value of σ. The model vertical resolution is defined by a list of values between zero and one that do not necessarily have to be evenly spaced. Commonly the resolution in the boundary layer is much finer than above, and the number of levels may vary upon the user demand.

The horizontal grid has an Arakawa-Lamb B-staggering of the velocity variables with respect to the scalar variables. This is shown in Figure 2 where it can be seen that the scalars (T, q, p, etc) are defined at the center of the grid box, while the eastward (u) and northward (v) velocity components are collocated at the corners. The center points of grid squares will be referred to as cross points, and the corner points are dot points. Hence horizontal velocity is defined at dot points. Data is input to the model, the preprocessors do the necessary interpolation to assure consistency with the grid.

All the above variables are defined in the middle of each model vertical layer, referred to as half-levels and represented by the dashed lines in Figure 1. Vertical velocity is carried at the full levels (solid lines). In defining the sigma levels it is the full levels that are listed, including levels at $\sigma = 0$ and 1. The number of model layers is therefore always one less than the number of full sigma levels.

The finite differencing in the model is, of course, crucially dependent upon the grid staggering wherever gradients or averaging are represented terms in the equation.

1.3 Map Projections and Map-Scale Factors

The modeling system has a choice of four map projections. Lambert Conformal is suitable for mid-latitudes, Polar Stereographic for high latitudes, Normal Mercator for low latitudes, and Rotated Mercator for extra choice. The *x* and *y* directions in the model do not correspond to west-east and north-south except for the Normal Mercator projection, and therefore the observed wind generally has to be rotated to the model grid, and the model *u* and *v* components need to be rotated before comparison with observations. These transformations are accounted for in the model pre-processors that provide data on the model grid (Please note that model output of u and v components, raw or postprocessed, should be rotated to a lat/lon grid before comparing to observations). The map scale factor, *m*, is defined by

m = (distance on grid) / (actual distance on earth)

and its value is usually close to one, varying with latitude. The projections in the model preserve the shape of small areas, so that dx=dy everywhere, but the grid length varies across the domain to allow a representation of a spherical surface on a plane surface. Map-scale factors need to be accounted for in the model equations wherever horizontal gradients are used.

2 Model Description

2.1 Dynamics

The model dynamic equations and numerical discretization are described by *Grell et al.* [1994].
Horizontal Momentum Equations

$$\frac{\partial p^* u}{\partial t} = -m^2 \left(\frac{\partial p^* uu/m}{\partial x} + \frac{\partial p^* vu/m}{\partial y} \right) - \frac{\partial p^* u\dot{\sigma}}{\partial \sigma}$$
$$-mp^* \left[\frac{RT_v}{(p^* + p_t/\sigma)} \frac{\partial p^*}{\partial x} + \frac{\partial \phi}{\partial x} \right] + fp^* v + F_H u + F_V u, \tag{2}$$

$$\frac{\partial p^* v}{\partial t} = -m^2 \left(\frac{\partial p^* uv/m}{\partial x} + \frac{\partial p^* vv/m}{\partial y} \right) - \frac{\partial p^* v\dot{\sigma}}{\partial \sigma}$$
$$-mp^* \left[\frac{RT_v}{(p^* + p_t/\sigma)} \frac{\partial p^*}{\partial y} + \frac{\partial \phi}{\partial y} \right] + fp^* u + F_H v + F_V v, \tag{3}$$

where u and v are the eastward and northward components of velocity, T_v is virtual temperature, ϕ is geopotential height, f is the coriolis parameter, R is the gas constant for dry air, m is the map scale factor for either the Polar Stereographic, Lambert Conformal, or Mercator map projections, $\dot{\sigma} = \frac{d\sigma}{dt}$, and F_H and F_V represent the effects of horizontal and vertical diffusion, and $p^* = p_s - p_t$.

Continuity and Sigmadot $(\dot{\sigma})$ Equations

$$\frac{\partial p^*}{\partial t} = -m^2 \left(\frac{\partial p^* u/m}{\partial x} + \frac{\partial p^* v/m}{\partial y} \right) - \frac{\partial p^* \dot{\sigma}}{\partial \sigma}. \tag{4}$$

The vertical integral of Equation 4 is used to compute the temporal variation of the surface pressure in the model,

$$\frac{\partial p^*}{\partial t} = -m^2 \int_0^1 \left(\frac{\partial p^* u/m}{\partial x} + \frac{\partial p^* v/m}{\partial y} \right) d\sigma. \tag{5}$$

After calculation of the surface-pressure tendency $\frac{\partial p^*}{\partial t}$, the vertical velocity in sigma coordinates $(\dot{\sigma})$ is computed at each level in the model from the vertical integral of Equation 4.

$$\dot{\sigma} = -\frac{1}{p^*} \int_0^\sigma \left[\frac{\partial p^*}{\partial t} + m^2 \left(\frac{\partial p^* u/m}{\partial x} + \frac{\partial p^* v/m}{\partial y} \right) \right] d\sigma\prime, \tag{6}$$

where $\sigma\prime$ is a dummy variable of integration and $\dot{\sigma}(\sigma = 0) = 0$.

Thermodynamic Equation and Equation for Omega (ω)
The thermodynamic equation is

$$\frac{\partial p^* T}{\partial t} = -m^2 \left(\frac{\partial p^* uT/m}{\partial x} + \frac{\partial p^* vT/m}{\partial y} \right) - \frac{\partial p^* T\dot{\sigma}}{\partial \sigma} + \frac{RT_v \omega}{c_{pm}(\sigma + P_t/p_{ast})} + \frac{p^* Q}{c_{pm}} + F_H T + F_V T, \tag{7}$$

where c_{pm} is the specific heat for moist air at constant pressure, Q is the diabatic heating, $F_H T$ represents the effect of horizontal diffusion, $F_V T$ represents the effect of vertical mixing and dry convective adjustment, and ω is

$$\omega = p^* \dot{\sigma} + \sigma \frac{dp^*}{dt}, \tag{8}$$

where,

$$\frac{dp^*}{dt} = \frac{\partial p^*}{\partial t} + m \left(u \frac{\partial p^*}{\partial x} + v \frac{\partial p^*}{\partial y} \right). \tag{9}$$

The expression for $c_{pm} = c_p(1 + 0.8q_v)$,
where c_p is the specific heat at constant pressure for dry air and q_v is the mixing ratio of water vapor.

Hydrostatic Equation
The hydrostatic equation is used to compute the geopotential heights from the virtual temperature T_v,

$$\frac{\partial \phi}{\partial ln(\sigma + p_t/p^*)} = -RT_v \left[1 + \frac{q_c + q_r}{1 + q_v} \right]^{-1}, \tag{10}$$

where $T_v = T(1 + 0.608q_v)$, q_v, q_c, and q_r are the water vapor, cloud water or ice, and rain water or snow, mixing ratios.

2.2 Physics

2.2.1 Radiation Scheme

RegCM4 uses the radiation scheme of the NCAR CCM3, which is described in *Kiehl et al.* [1996]. Briefly, the solar component, which accounts for the effect of O_3, H_2O, CO_2, and O_2, follows the δ-Eddington approximation of *Kiehl et al.* [1996]. It includes 18 spectral intervals from 0.2 to 5 μm. The cloud scattering and absorption parameterization follow that of *Slingo* [1989], whereby the optical properties of the cloud droplets (extinction optical depth, single scattering albedo, and asymmetry parameter) are expressed in terms of the cloud liquid water content and an effective droplet radius. When cumulus clouds are formed, the gridpoint fractional cloud cover is such that the total cover for the column extending from the model-computed cloud-base level to the cloud-top level (calculated assuming random overlap) is a function of horizontal gridpoint spacing. The thickness of the cloud layer is assumed to be equal to that of the model layer, and a different cloud water content is specified for middle and low clouds.

2.2.2 Land Surface Models

BATS (default): BATS is a surface package designed to describe the role of vegetation and interactive soil moisture in modifying the surface-atmosphere exchanges of momentum, energy, and water vapor (see *Dickinson et al.* [1993] for details). The model has a vegetation layer, a snow layer, a surface soil layer, 10 cm thick, or root zone layer, 1-2 m thick, and a third deep soil layer 3 m thick. Prognostic equations are solved for the soil layer temperatures using a generalization of the force-restore method of *Deardoff* [1978]. The temperature of the canopy and canopy foilage is calculated diagnostically via an energy balance formulation including sensible, radiative, and latent heat fluxes.

The soil hydrology calculations include predictive equations for the water content of the soil layers. These equations account for precipitation, snowmelt, canopy foiliage drip, evapotranspiration, surface runoff, infiltration below the root zone, and diffusive exchange of water between soil layers. The soil water movement formulation is obtained from a fit to results from a high-resolution soil model Dic [1984] and the surface runoff rates are expressed as functions of the precipitation rates and the degree of soil water saturation. Snow depth is prognostically calculated from snowfall, snowmelt, and sublimation. Precipitation is assumed to fall in the form of snow if the temperature of the lowest model level is below 271 K.

Sensible heat, water vapor, and momentum fluxes at the surface are calculated using a standard surface drag coefficient formulation based on surface-layer similarity theory. The drag coefficient depends on the surface roughness length and on the atmospheric stability in the surface layer. The surface evapotranspiration rates depend on the availability of soil water. Biosphere-Atmosphere Transfer Scheme (BATS) has 20 vegetation types (Table 2; soil textures ranging from coarse (sand), to intermediate (loam), to fine (clay); and different soil colors (light to dark) for the soil albedo calculations. These are described in *Dickinson et al.* [1986].

In the latest release version, additional modifications have been made to BATSin order to account for the subgrid variability of topography and landcover using a mosaic-type approach [*Giorgi et al.*, 2003a]. Thismodification adopts a regular fine-scale surface subgrid for eachcoarse model grid cell. Meteorological variables are disaggregatedfrom the coarse grid to the fine grid based on the elevationdifferences. The BATS calculations are then performed separatelyfor each subgrid cell, and surface fluxes are reaggregated onto thecoarse grid cell for input to the atmospheric model. Thisparameterization showed a marked improvement in the representation ofthe surface hydrological cycle in mountainous regions [*Giorgi et al.*, 2003a].

CLM (optional): The Community Land Model (CLM; *Oleson et al.* [2008]) is the land surface model developed by the National Center of Atmospheric Research (NCAR) as part of the Community Climate System Model (CCSM), described in detail in *Collins et al.* [2006]. CLM version 3.5 was coupled to RegCM for a more detailed land surface description option. CLM contains five possible snow layers with an additional representation of trace snow and ten unevenly spaced soil layers with explicit solutions of temperature, liquid water and ice water in each layer. To account for land surface complexity within a climate model grid cell, CLM uses a tile or mosaic approach to capture surface heterogeneity. Each CLM gridcell contains up to four different land cover types (glacier, wetland, lake, and vegetated), where the vegetated fraction can be further divided into 17 different plant functional types. Hydrological and energy balance equations are solved for each land cover type and aggregated back to the gridcell level. A detailed discussion of CLM version 3 implemented in RegCM3 and comparative analysis of land surface parameterization options is presented in *Steiner et al.* [2009]. Since CLM was developed for the global scale,

Table 1: Land Cover/Vegetation classes

1.	Crop/mixed farming
2.	Short grass
3.	Evergreen needleleaf tree
4.	Deciduous needleleaf tree
5.	Deciduous broadleaf tree
6.	Evergreen broadleaf tree
7.	Tall grass
8.	Desert
9.	Tundra
10.	Irrigated Crop
11.	Semi-desert
12.	Ice cap/glacier
13.	Bog or marsh
14.	Inland water
15.	Ocean
16.	Evergreen shrub
17.	Deciduous shrub
18.	Mixed Woodland
19.	Forest/Field mosaic
20.	Water and Land mixture

several input files and processes were modified to make it more appropriate for regional simulations, including (1) the use of high resolution input data, (2) soil moisture initialization, and (3) and an improved treatment of grid cells along coastlines. For the model input data, CLM requires several time-invariant surface input parameters: soil color, soil texture, percent cover of each land surface type, leaf and stem area indices, maximum saturation fraction, and land fraction [*Lawrence and Chase*, 2007]. Table 3 shows the resolution for each input parameter used at the regional scale in RegCM-CLM compared to resolutions typically used for global simulations. The resolution of surface input parameters was increased for several parameters to capture surface heterogeneity when interpolating to the regional climate grid. Similar to *Lawrence and Chase* [2007], the number of soil colors was extended from 8 to 20 classes to resolve regional variations. The second modification was to update the soil moisture initialization based on a climatological soil moisture average [*Giorgi and Bates*, 1989] over the use of constant soil moisture content throughout the grid generally used for global CLM. By using a climatological average for soil moisture, model spin-up time is reduced with regards to deeper soil layers. The third modification to the CLM is the inclusion of a mosaic approach for gridcells that contain both land and ocean surface types. With this approach, a weighted average of necessary surface variables was calculated for land/ocean gridcells using the land fraction input dataset. This method provides a better representation of coastlines using the high-resolution land fraction data described in Table 3. For a more detailed description of CLM physics parameterizations see *Oleson* [2004].

Table 2: BATS vegetation/land-cover

Parameter	Land Cover/Vegetation Type																			
	1	2	3	4	5	6	7	8	9	10	11	12	13	14	15	16	17	18	19	20
Max fractional vegetation cover	0.85	0.80	0.80	0.80	0.80	0.90	0.80	0.00	0.60	0.80	0.35	0.00	0.80	0.00	0.00	0.80	0.80	0.80	0.80	0.80
Difference between max fractional vegetation cover and cover at 269 K	0.6	0.1	0.1	0.3	0.5	0.3	0.0	0.2	0.6	0.1	0.0	0.4	0.0	0.0	0.2	0.3	0.2	0.4	0.4	
Roughness length (m)	0.08	0.05	1.00	1.00	0.80	2.00	0.10	0.05	0.04	0.06	0.10	0.01	0.03	0.0004	0.0004	0.10	0.10	0.80	0.3	0.3
Displacement height (m)	0.0	0.0	9.0	9.0	0.0	18.0	0.0	0.0	0.0	0.0	0.0	0.0	0.0	0.0	0.0	0.0	0.0	0.0	0.0	0.0
Min stomatal resistence (s/m)	45	60	80	80	120	60	60	200	80	45	150	200	45	200	200	80	120	100	120	120
Max Leaf Area Index	6	2	6	6	6	6	6	0	6	6	6	0	6	0	0	6	6	6	6	6
Min Leaf Area Index	0.5	0.5	5	1	1	5	0.5	0	0.5	0.5	0.5	0	0.5	0	0	5	1	3	0.5	0.5
Stem (dead matter area index)	0.5	4.0	2.0	2.0	2.0	2.0	2.0	0.5	0.5	2.0	2.0	2.0	2.0	2.0	2.0	2.0	2.0	2.0	2.0	2.0
Inverse square root of leaf dimension ($m^{-1/2}$)	10	5	5	5	5	5	5	5	5	5	5	5	5	5	5	5	5	5	5	5
Light sensitivity factor (m^2 W^{-1})	0.02	0.02	0.06	0.06	0.06	0.06	0.02	0.02	0.02	0.02	0.02	0.02	0.02	0.02	0.02	0.02	0.02	0.06	0.02	0.02
Upper soil layer depth (mm)	100	100	100	100	100	100	100	100	100	100	100	100	100	100	100	100	100	100	100	100
Root zone soil layer depth (mm)	1000	1000	1500	1500	2000	1500	1000	1000	1000	1000	1000	1000	1000	1000	1000	1000	1000	2000	2000	2000
Depth of total soil (mm)	3000	3000	3000	3000	3000	3000	3000	3000	3000	3000	3000	3000	3000	3000	3000	3000	3000	3000	3000	3000
Soil texture type	6	6	6	6	7	8	6	3	6	6	5	12	6	6	6	6	5	6	6	0
Soil color type	5	3	4	4	4	4	4	1	3	3	2	1	5	5	5	4	3	4	4	0
Vegetation albedo for wavelengths $< 0.7\ \mu$ m	0.10	0.10	0.05	0.05	0.08	0.04	0.08	0.20	0.10	0.08	0.17	0.80	0.06	0.07	0.07	0.05	0.08	0.06	0.06	0.06
Vegetation albedo for wavelengths $> 0.7\ \mu$ m	0.30	0.30	0.23	0.23	0.28	0.20	0.30	0.40	0.30	0.28	0.34	0.60	0.18	0.20	0.20	0.23	0.28	0.24	0.18	0.18

Table 3: Resolution for CLM input parameters

Input data	Grid Spacing	Lon range	Lat range
Glacier	0.05° x 0.05°	±179.975	±89.975
Lake	0.05° x 0.05°	±179.975	±89.975
Wetland	0.05° x 0.05°	±179.975	±89.975
Land fraction	0.05° x 0.05°	±179.975	±89.975
LAI/SAI	0.5° x 0.5°	±179.75	±89.75
PFT	0.5° x 0.5°	±179.75	±89.75
Soil color	0.05° x 0.05°	±179.975	±89.975
Soil texture	0.05° x 0.05°	±179.975	±89.975
Max. sat. area	0.5° x 0.5°	±179.75	±89.75

2.2.3 Planetary Boundary Layer Scheme

The planetary boundary layer scheme, developed by *Holtslag et al.* [1990], is based on a nonlocal diffusion concept that takes into account countergradient fluxes resulting from large-scale eddies in an unstable, well-mixed atmosphere. The vertical eddy flux within the PBL is given by

$$F_c = -K_c \left(\frac{\partial C}{\partial z} - \gamma_c \right) \tag{11}$$

where γ_c is a "countergradient" transport term describing nonlocal transport due to dry deep convection. The eddy diffusivity is given by the nonlocal formulation

$$K_c = k w_t z \left(1 - \frac{z}{h}^2 \right), \tag{12}$$

where k is the von Karman constant; w_t is a turbulent convective velocity that depends on the friction velocity, height, and the Monin–Obhukov length; and h is the PBL height. The countergradient term for temperature and water vapor is given by

$$\gamma_c = C \frac{{\phi_c}^0}{w_t h}, \tag{13}$$

where C is a constant equal to 8.5, and ${\phi_c}^0$ is the surface temperature or water vapor flux. Equation 13 is applied between the top of the PBL and the top of the surface layer, which is assumed to be equal to $0.1h$. Outside this region and for momentum, γ_c is assumed to be equal to 0.

For the calculation of the eddy diffusivity and countergradient terms, the PBL height is diagnostically computed from

$$h = \frac{\mathrm{Ri_c r}[u(h)^2 + v(h)^2]}{(g/\theta_s)[\theta_v(h) - \theta_s]} \tag{14}$$

where $u(h)$, $v(h)$, and θ_v are the wind components and the virtual potential temperature at the PBL height, g is gravity, $\mathrm{Ri_c r}$ is the critical bulk Richardson number, and θ_s is an appropriate temperature of are near the surface. Refer to *Holtslag et al.* [1990] and *Holtslag and Boville* [1993] for a more detailed description.

2.2.4 Convective Precipitation Schemes

Convective precipitation is computed using one of three schemes: (1) Modified-Kuo scheme *Anthes* [1977]; (2) Grell scheme *Grell* [1993]; and (3) MIT-Emanuel scheme [*Emanuel*, 1991; *Emanuel and Zivkovic-Rothman*, 1999].

In addition, the Grell parameterization is implemented using one of two closure assumptions: (1) the Arakawa and Schubert closure *Grell et al.* [1994] and (2) the Fritsch and Chappell closure *Fritsch and Chappell* [1980], hereafter refered to as AS74 and FC80, respectively.

1. Kuo Scheme: Convective activity in the Kuo scheme is initiated when the moisture convergence M in a column exceeds a given threshold and the vertical sounding is convectively unstable. A fraction of the moisture convergence β moistens the column and the rest is converted into rainfall P^{CU} according to the following relation:

$$P^{CU} = M(1-\beta). \tag{15}$$

β is a function of the average relative humidity $\overline{RH}$ of the sounding as follows:

$$\beta = \begin{cases} 2(1-\overline{RH}) & \overline{RH} \geq 0.5 \\ 1.0 & \text{otherwise} \end{cases} \tag{16}$$

Note that the moisture convergence term includes only the advective tendencies for water vapor. However, evapotranspiration from the previous time step is indirectly included in M since it tends to moisten the lower atmosphere. Hence, as the evapotranspiration increases, more and more of it is converted into rainfall assuming the column is unstable. The latent heating resulting from condensation is distributed between the cloud top and bottom by a function that allocates the maximum heating to the upper portion of the cloud layer. To eliminate numerical point storms, a horizontal diffusion term and a time release constant are included so that the redistributions of moisture and the latent heat release are not performed instantaneously [*Giorgi and Bates*, 1989; *Giorgi and Marinucci*, 1991].

2. Grell Scheme: The Grell scheme *Grell* [1993], similar to the AS74 parameterization, considers clouds as two steady-state circulations: an updraft and a downdraft. No direct mixing occurs between the cloudy air and the environmental air except at the top and bottom of the circulations. The mass flux is constant with height and no entrainment or detrainment occurs along the cloud edges. The originating levels of the updraft and downdraft are given by the levels of maximum and minimum moist static energy, respectively. The Grell scheme is activated when a lifted parcel attains moist convection. Condensation in the updraft is calculated by lifting a saturated parcel. The downdraft mass flux (m_0) depends on the updraft mass flux (m_b) according to the following relation:

$$m_0 = \frac{\beta I_1}{I_2} m_b, \tag{17}$$

where I_1 is the normalized updraft condensation, I_2 is the normalized downdraft evaporation, and β is the fraction of updraft condensation that re-evaporates in the downdraft. β depends on the wind shear and typically varies between 0.3 and 0.5. Rainfall is given by

$$P^{CU} = I_1 m_b (1-\beta). \tag{18}$$

Heating and moistening in the Grell scheme are determined both by the mass fluxes and the detrainment at the cloud top and bottom. In addition, the cooling effect of moist downdrafts is included.

Due to the simplistic nature of the Grell scheme, several closure assumptions can be adopted. RegCM4's earlier version directly implements the quasi-equilibrium assumption of AS74. It assumes that convective clouds stabilize the environment as fast as non-convective processes destabilize it as follows:

$$m_b = \frac{ABE'' - ABE}{NA\Delta t}, \tag{19}$$

where ABE is the buoyant energy available for convection, ABE'' is the amount of buoyant energy available for convection in addition to the buoyant energy generated by some of the non-convective processes during the time interval Δt, and NA is the rate of change of ABE per unit m_b. The difference $ABE'' - ABE$ can be thought of as the rate of destabilization over time Δt. ABE'' is computed from the current fields plus the future tendencies resulting from the advection of heat and moisture and the dry adiabatic adjustment.

In the latest RegCM4 version, by default, we use a stability based closure assumption, the FC80 type closure assumption, that is commonly implemented in GCMs and RCMs. In this closure, it is assumed that convection removes the ABE over a given time scale as follows:

$$m_b = \frac{ABE}{NA\tau}, \tag{20}$$

where τ is the *ABE* removal time scale.

The fundamental difference between the two assumptions is that the AS74 closure assumption relates the convective fluxes and rainfall to the tendencies in the state of the atmosphere, while the FC80 closure assumption relates the convective fluxes to the degree of instability in the atmosphere. Both schemes achieve a statistical equilibrium between convection and the large-scale processes.

3. MIT-Emanuel scheme: The newest cumulus convection option to the REGional Climate Model version 4 (RegCM4) is theMassachusetts Institute of Technology (MIT) scheme. More detailed descriptions can be found in *Emanuel* [1991] and*Emanuel and Zivkovic-Rothman* [1999]. The scheme assumes that the mixing in clouds ishighly episodic and inhomogeneous (as opposed to a continuousentraining plume) and considers convective fluxes based on anidealized model of sub-cloud-scale updrafts and downdrafts.Convection is triggered when the level of neutral buoyancy is greaterthan the cloud base level. Between these two levels, air is liftedand a fraction of the condensed moisture forms precipitation while theremaining fraction forms the cloud. The cloud is assumed to mix withthe air from the environment according to a uniform spectrum ofmixtures that ascend or descend to their respective levels of neutralbuoyancy. The mixing entrainment and detrainment rates are functionsof the vertical gradients of buoyancy in clouds. The fraction of thetotal cloud base mass flux that mixes with its environment at eachlevel is proportional to the undiluted buoyancy rate of change withaltitude. The cloud base upward mass flux is relaxed towards thesub-cloud layer quasi equilibrium.

In addition to a more physical representation of convection, theMIT-Emanuel scheme offers several advantages compared to theother RegCM4 convection options. For instance, it includes aformulation of the auto-conversion of cloud water into precipitationinside cumulus clouds, and ice processes are accounted for by allowingthe auto-conversion threshold water content to be temperaturedependent. Additionally, the precipitation is added to a single,hydrostatic, unsaturated downdraft that transports heat and water.Lastly, the MIT-Emanuel scheme considers the transport of passive tracers.

2.2.5 Large-Scale Precipitation Scheme

Subgrid Explicit Moisture Scheme (SUBEX) is used to handle nonconvective clouds and precipitation resolved by the model. This is one of the new components of the model. SUBEX accounts for the subgrid variability in clouds by linking the average grid cell relative humidity to the cloud fraction and cloud water following the work of *Sundqvist et al.* [1989].

The fraction of the grid cell covered by clouds, FC, is determined by,

$$FC = \sqrt{\frac{RH - RH_{min}}{RH_{max} - RH_{min}}} \tag{21}$$

where RH_{min} is the relative humidity threshold at which clouds begin to form, and RH_{max} is the relative humidity where FC reaches unity. FC is assumed to be zero when RH is less than RH_{min} and unity when RH is greater than RH_{max}.

Precipitation P forms when the cloud water content exceeds the autoconversion threshold ${Q^{th}}_c$ according to the following relation:

$$P = C_{ppt}(Q_c/FC - {Q_c}^{th})FC \tag{22}$$

where $1/C_{ppt}$ can be considered the characteristic time for which cloud droplets are converted to raindrops. The threshold is obtained by scaling the median cloud liquid water content equation according to the following:

$${Q^{th}}_c = C_{acs}10^{-0.49+0.013T}, \tag{23}$$

where T is temperature in degrees Celsius, and C_{acs} is the autoconversion scale factor. Precipitation is assumed to fall instantaneously.

SUBEX also includes simple formulations for raindrop accretion and evaporation. The formulation for the accretion of cloud droplets by falling rain droplets is based on the work of *Beheng* [1994] and is as follows:

$$P_{acc} = C_{acc}QP_{sum} \tag{24}$$

where P_{acc} is the amount of accreted cloud water, C_{acc} is the accretion rate coefficient, and P_{sum} is the accumulated precipitation from above falling through the cloud.

Precipitation evaporation is based on the work of *Sundqvist et al.* [1989] and is as follows,

$$P_{evap} = C_{evap}(1 - RH)P^{1/2}{}_{sum} \tag{25}$$

where P_{evap} is the amount of evaporated precipitation, and C_{evap} is the rate coefficient. For a more detailed description of SUBEX and a list of the parameter values refer to *Pal et al.* [2000].

2.2.6 Ocean flux Parameterization

1. BATS: BATS uses standard Monin-Obukhov similarity relations to compute the fluxes with no special treatment of convective and very stable conditions. In addition, the roughness length is set to a constant, i.e. it is not a function of wind and stability.
2. Zeng: The Zeng scheme describes all stability conditions and includes a gustiness velocity to account for the additional flux induced by boundary layer scale variability. Sensible heat (SH), latent heat (LH), and momentum (τ) fluxes between the sea surface and lower atmosphere are calculated using the following bulk aerodynamic algorithms,

$$\tau = \rho_a {u_*}^2 ({u_x}^2 + {u_y}^2)^{1/2}/u \tag{26}$$

$$\mathrm{SH} = -\rho_a C_{pa} u_* \theta_* \tag{27}$$

$$\mathrm{LH} = -\rho_a L_e u_* q_* \tag{28}$$

where u_x and u_y are mean wind components, u_* is the frictional wind velocity, θ_* is the temperature scaling parameter, q_* is the specific humidity scaling parameter, ρ_a is air density, C_{pa} is specific heat of air, and L_e is the latent heat of vaporization. For further details on the calculation of these parameters refer to *Zeng et al.* [1998].

2.2.7 Prognostic Sea Surface Skin Temperature Scheme

RegCM4 contains a option which allows for the computation of sea surface skin temperature as a prognostic variable following the scheme of *Zeng* [2005]. This allows for a realistic representation of the diurnal sea surface skin temperature, leading to improvements in the surface fluxes thus air-sea interactions. The scheme is based on a two-layer model which includes warm layer/cool skin effects as described by *Fairall et al.*). Temperatures in the two layers are calculated using a one-dimensional heat transfer equation and boundary conditions determined by surface to atmosphere fluxes (latent, sensible and radiative) and a 3 m depth sea surface temperature taken from the prescribed SSTs.

2.2.8 Pressure Gradient Scheme

Two options are available for calculating the pressure gradient force. The normal way uses the full fields. The other way is the hydrostatic deduction scheme which makes use of a perturbation temperature. In this scheme, extra smoothing on the top is done in order to reduce errors related to the PGF calculation.

2.2.9 Lake Model

The lake model developed by *Hostetler et al.* [1993] can be interactively coupled to the atmospheric model. In the lake model, fluxes of heat, moisture, and momentum are calculated based on meteorological inputs and the lake surface temperature and albedo. Heat is transferred vertically between lake model layers by eddy and convective mixing. Ice and snow may cover part or all of the lake surface.

In the lake model, the prognostic equation for temperature is,

$$\frac{\partial T}{\partial t} = (k_e + k_m)\frac{\partial^2 T}{\partial z^2} \tag{29}$$

where T is the temperature of the lake layer, and k_e and k_m are the eddy and molecular diffusivities, respectively. The parameterization of *Henderson-Sellers* [1986] is used to calculate k_e and k_m is set to a constant value of $39 \times 10^{-7}\ m^2\ s^{-1}$ except under ice and at the deepest points in the lake.

Sensible and latent heat fluxes from the lake are calculated using the BATS parameterizations *Dickinson et al.* [1993]. The bulk aerodynamic formulations for latent heat flux (F_q) and sensible heat flux (F_s) are as follows,

$$F_q = \rho_a C_D V_a (q_s - q_a) \tag{30}$$

$$F_s = \rho_a C_p C_D V_a (T_s - T_a) \tag{31}$$

where the subscripts *s* and *a* refer to surface and air, respectively; ρ_a is the density of air, V_a is the wind speed, C_p, q is specific humidity, and T is temperature. The momentum drag coefficient, C_D, depends on roughness length and the surface bulk Richardson number.

Under ice-free conditions, the lake surface albedo is calculated as a function of solar zenith angle *Henderson-Sellers* [1986]. Longwave radiation emitted from the lake is calculated according to the Stefan-Boltzmann law. The lake model uses the partial ice cover scheme of *Patterson and Hamblin* [1988] to represent the different heat and moisture exchanges between open water and ice surfaces and the atmosphere, and to calculate the surface energy of lake ice and overlying snow. For further details refer to *Hostetler et al.* [1993] and *Small and Sloan* [1999].

2.2.10 Aerosols and Dust (Chemistry Model)

The representation of dust emission processes is a key element in a dust model and depends on the wind conditions, the soil characteristics and the particle size. Following Marticorena and Bergametti (1995) and Alfaro and Gomes (2001), here the dust emission calculation is based on parameterizations of soil aggregate saltation and sandblasting processes. The main steps in this calculation are: The specification of soil aggregate size distribution for each model grid cell, the calculation of a threshold friction velocity leading to erosion and saltation processes, the calculation of the horizontal saltating soil aggregate mass flux, and finally the calculation of the vertical transportable dust particle mass flux generated by the saltating aggregates. In relation to the BATS interface, these parameterizations become effective in the model for cells dominated by desert and semi desert land cover.

References

Climate Processes and Climate Sensitivity, chap. Modeling evapotranspiration processes for three-dimensional global climate models, pp. 52–72, American Geophysical Union, 1984.

Anthes, R. A., A cumulus parameterization scheme utilizing a one-dimensional cloud model, *Mon. Wea. Rev.*, *105*, 270–286, 1977.

Beheng, K. D., A parameterization of warm cloud microphysical conversion processes, *Atmos. Res.*, *33*, 193–206, 1994.

Briegleb, B. P., Delta-eddington approximation for solar radiation in the ncar community climate model, *J. Geophys. Res.*, *97*, 7603–7612, 1992.

Collins, W. D., et al., The Community Climate System Model version 3 (CCSM3), *Journal of Climate*, *19*, 2122–2143, 2006.

Deardoff, J. W., Efficient prediction of ground surface temperature and moisture with inclusion of a layer of vegetation, *J. Geophys. Res.*, *83*, 1889–1903, 1978.

Dickinson, R. E., P. J. Kennedy, A. Henderson-Sellers, and M. Wilson, Biosphere-atmosphere transfer scheme (bats) for the ncar community climate model, *Tech. Rep. NCARE/TN-275+STR*, National Center for Atmospheric Research, 1986.

Dickinson, R. E., R. M. Errico, F. Giorgi, and G. T. Bates, A regional climate model for the western United States, *Climatic Change*, *15*, 383–422, 1989.

Dickinson, R. E., A. Henderson-Sellers, and P. J. Kennedy, Biosphere-atmosphere transfer scheme (bats) version 1e as coupled to the ncar community climate model, *Tech. rep.*, National Center for Atmospheric Research, 1993.

Emanuel, K. A., A scheme for representing cumulus convection in large-scale models, *J. Atmos. Sci.*, *48*(21), 2313–2335, 1991.

Emanuel, K. A., and M. Zivkovic-Rothman, Development and evaluation of a convection scheme for use in climate models, *J. Atmos. Sci.*, *56*, 1766–1782, 1999.

Fairall, C., E. Bradley, J. Godfrey, G. Wick, J. Edson, and G. Young, Cool-skin and warm layer effects on sea surface temperature, *Journal of Geophysical Research*, *101*, 1295–1308.

Fritsch, J. M., and C. F. Chappell, Numerical prediction of convectively driven mesoscale pressure systems. part i: Convective parameterization, *J. Atmos. Sci.*, *37*, 1722–1733, 1980.

Giorgi, F., Two-dimensional simulations of possible mesoscale effects of nuclear war fires, *J. Geophys. Res.*, *94*, 1127–1144, 1989.

Giorgi, F., Simulation of regional climate using a limited area model nested in a general circulation model, *J. Climate*, *3*, 941–963, 1990.

Giorgi, F., and G. T. Bates, The climatological skill of a regional model over complex terrain, *Mon. Wea. Rev.*, *117*, 2325–2347, 1989.

Giorgi, F., and M. R. Marinucci, Validation of a regional atmospheric model over europe: Sensitivity of wintertime and summertime simulations to selected physics parameterizations and lower boundary conditions, *Quart. J. Roy. Meteor. Soc.*, *117*, 1171–1206, 1991.

Giorgi, F., G. T. Bates, and S. J. Nieman, The multi-year surface climatology of a regional atmospheric model over the western united states, *J. Climate*, *6*, 75–95, 1993a.

Giorgi, F., M. R. Marinucci, and G. T. Bates, Development of a second generation regional climate model (regcm2) i: Boundary layer and radiative transfer processes, *Mon. Wea. Rev.*, *121*, 2794–2813, 1993b.

Giorgi, F., X. Q. Bi, and Y. Qian, Indirect vs. direct effects of anthropogenic sulfate on the climate of east asia as simulated with a regional coupled climate-chemistry/aerosol model, *Climatic Change*, *58*, 345–376, 2003a.

Giorgi, F., R. Francisco, and J. S. Pal, Effects of a subgrid-scale topography and land use scheme on the simulation of surface climate and hydrology. part 1: Effects of temperature and water vapor disaggregation., *Journal of Hydrometeorology*, *4*, 317–333, 2003b.

Grell, G., Prognostic evaluation of assumptions used by cumulus parameterizations, *Mon. Wea. Rev.*, *121*, 764–787, 1993.

Grell, G. A., J. Dudhia, and D. R. Stauffer, Description of the fifth generation Penn State/NCAR Mesoscale Model (MM5), *Tech. Rep. TN-398+STR*, NCAR, Boulder, Colorado, pp. 121, 1994.

Hack, J. J., B. A. Boville, B. P. Briegleb, J. T. Kiehl, P. J. Rasch, and D. L. Williamson, Description of the ncar community climate model (ccm2), *Tech. Rep. NCAR/TN-382+STR*, National Center for Atmospheric Research, 1993.

Henderson-Sellers, B., Calculating the surface energy balance for lake and reservoir modeling: A review, *Rev. Geophys.*, *24*(3), 625–649, 1986.

Holtslag, A. A. M., and B. A. Boville, Local versus nonlocal boundary-layer diffusion in a global climate model, *J. Climate*, *6*, 1993.

Holtslag, A. A. M., E. I. F. de Bruijn, and H.-L. Pan, A high resolution air mass transformation model for short-range weather forecasting, *Mon. Wea. Rev.*, *118*, 1561–1575, 1990.

Hostetler, S. W., G. T. Bates, and F. Giorgi, Interactive nesting of a lake thermal model within a regional climate model for climate change studies, *Geophysical Research*, *98*, 5045–5057, 1993.

Hsie, E. Y., R. A. Anthes, and D. Keyser, Numerical simulation of frontogenisis in a moist atmosphere, *J. Atmos. Sci.*, *41*, 2581–2594, 1984.

Kiehl, J. T., J. J. Hack, G. B. Bonan, B. A. Boville, B. P. Breigleb, D. Williamson, and P. Rasch, Description of the ncar community climate model (ccm3), *Tech. Rep. NCAR/TN-420+STR*, National Center for Atmospheric Research, 1996.

Lawrence, P., and T. Chase, Representing a new MODIS consistent land surface in the Community Land Model (CLM3.0), *J. Geophys. Res.*, *112*, g01023, 2007.

Oleson, K. e. a., Technical description of the Community Land Model (CLM), *Tech. Rep. Technical Note NCAR/TN-461+STR*, NCAR, 2004.

Oleson, K. W., et al., Improvements to the Community Land Model and their impact on the hydrological cycle, *Journal of Geophysical Research-Biogeosciences*, *113*(G1), 2008.

Pal, J. S., E. E. Small, and E. A. B. Eltahir, Simulation of regional-scale water and energy budgets: Representation of subgrid cloud and precipitation processes within RegCM, *J. Geophys. Res.-Atmospheres*, *105*(D24), 29,579–29,594, 2000.

Patterson, J. C., and P. F. Hamblin, Thermal simulation of a lake with winter ice cover, *Limn. Oceanography*, *33*, 323–338, 1988.

Slingo, J. M., A gcm parameterization for the shortwave radiative properties of water clouds, *J. Atmos. Sci.*, *46*, 1419–1427, 1989.

Small, E. E., and L. C. Sloan, Simulating the water balance of the aral sea with a coupled regional climate-lake model, *J. Geophys. Res.*, *104*, 6583–6602, 1999.

Steiner, A. L., J. S. Pal, S. A. Rauscher, J. L. Bell, N. S. Diffenbaugh, A. Boone, L. C. Sloan, and F. Giorgi, Land surface coupling in regional climate simulations of the West African monsoon, *Climate Dynamics*, *33*(6), 869–892, 2009.

Sundqvist, H., E. Berge, and J. E. Kristjansson, The effects of domain choice on summer precipitation simulation and sensitivity in a regional climate model, *J. Climate*, *11*, 2698–2712, 1989.

Zeng, X., A prognostic scheme of sea surface skin temperature for modeling and data assimilation, *Geophysical Research Letters*, *32*, l14605, 2005.

Zeng, X., M. Zhao, and R. E. Dickinson, Intercomparison of bulk aerodynamic algoriths for the computation of sea surface fluxes using toga coare and tao data, *J. Climate*, *11*, 2628–2644, 1998.

BATS Biosphere-Atmosphere Transfer Scheme

BATS1e Biosphere-Atmosphere Transfer Scheme version 1e

CAM Community Atmosphere Model

CAPE convective available potential energy

CCM Community Climate Model

CCM1 Community Climate Model version 1

CCM2 Community Climate Model version 2

CCM3 Community Climate Model version 3

CLM0 Common Land Model version 0

CLM2 Community Land Model version 2

CLM3 Community Land Model version 3

CMAP CPC Merged Analysis of Precipitation

CRU Climate Research Unit

CPC Climate Prediction Center

ECMWF European Centre for Medium-Range Weather Forecasts

ERA40 ECMWF 40-year Reanalysis

ESP Earth Systems Physics

FAO Food and Agriculture Organization of the United Nations

fvGCM NASA Data Assimilation Office atmospheric finite-volume general circulation model

GLCC Global Land Cover Characterization

GCM General Circulation Model

HadAM3H Hadley Centre Atmospheric Model version 3H

ICTP Abdus Salam International Centre for Theoretical Physics

IPCC Intergovernmental Panel on Climate Change

IBIS Integrated BIosphere Simulator

LAI leaf area index

LAMs limited area models

LBCs lateral boundary conditions

MC2 Mesoscale Compressible Community model

MIT Massachusetts Institute of Technology

MM4 Mesoscale Model version 4

MM5 Mesoscale Model version 5

MERCURE Modelling European Regional Climate Understanding and Reducing Errors

NNRP NCEP/NCAR Reanalysis Product

NNRP1 NCEP/NCAR Reanalysis Product version 1

NNRP2 NCEP/NCAR Reanalysis Product version 2

NCAR National Center for Atmospheric Research

NCEP National Centers for Environmental Prediction

PBL planetary boundary layer

PC Personal Computer

PIRCS Project to Intercompare Regional Climate Simulations

PFT plant functional type

PSU Pennsylvania State University

PWC Physics of Weather and Climate

RCM Regional Climate Model

RegCM REGional Climate Model

RegCM1 REGional Climate Model version 1

RegCM2 REGional Climate Model version 2

RegCM2.5 REGional Climate Model version 2.5

RegCM3 REGional Climate Model version 3

RegCM4 REGional Climate Model version 4

RegCNET REGional Climate Research NETwork

RMIP Regional Climate Model Intercomparison Project

SIMEX the Simple EXplicit moisture scheme

SST sea surface temperature

SUBEX the SUB-grid EXplicit moisture scheme

USGS United States Geological Survey

JJA June, July, and August

JJAS June, July, August, and September

JFM January, February, and March